

Synthesis of TiO₂ with diverse morphologies as supports of manganese catalysts for CO oxidation

Khadija Hedjazi¹  · Runduo Zhang¹ · Rong Cui¹ · Ning Liu¹ · Biaohua Chen¹

Received: 27 June 2015 / Accepted: 24 November 2015 / Published online: 16 December 2015
© The Author(s) 2015. This article is published with open access at Springerlink.com

Abstract The catalytic CO oxidation reaction has been investigated over a series of Mn/TiO₂ catalysts. The titanium dioxides, including several mesoporous structures were prepared by different synthesis procedures. The mesoporous TiO₂ synthesized using evaporation-induced self-assembly (EISA) method exhibited the highest surface area (217.14 m²/g). The successful loading of the active manganese component (2 %) to TiO₂ supports showed high dispersion of MnO_x species in amorphous state. Characterizations of XRD, N₂ adsorption–desorption, pore size distributions, TEM, H₂-TPR and XPS were applied to contrast their structure properties and correlated with the corresponding catalytic performance. The Mn/EISA exhibited the highest catalytic activity among the series of Mn/TiO₂ catalysts, which could completely oxidize CO into CO₂ at temperature as low as 270 °C, due to its highly ordered mesoporous channels, which effectively enlarge the surface area leading to promoting a strong interaction between MnO_x species (68 % Mn³⁺) and TiO₂ support.

Keywords Mesoporous · Anatase · Rutile · MnO_x · Oxidation

Introduction

Exhaust gas treatment has been the focus of current research for a wide array of applications. The main sources of air pollution, such as CO, have become serious problems

with the development of the social society. The catalytic oxidation is an effective way to eliminate harmful carbon monoxide and it is also a common probe reaction with one rate-determining stage and sole product. Titanium dioxides supports of manganese could be a good choice as catalyst due to their high chemical stability, satisfactory resistance to poisoning and simplify the system [1].

Manganese (Mn) is a transition metal that plays a fundamental role in many environmental reactions in the state of its oxides or ox-hydroxides [2–4]. The dominant oxidation states of Mn in the environment are II, III, and IV. Each oxidation state has different solubilities that can be linked to redox reactions associated with their aqueous/solid state partitioning [5]. A manganese nitrate precursor results primarily in crystal MnO₂, while a manganese acetate precursor results chiefly in a highly dispersed Mn₂O₃ surface. Supported Mn species are effective catalysts for low-temperature CO oxidation. Several studies have determined the use of Mn/TiO₂ catalyst [6], but there are limited references focusing on the analysis of the influence of diverse supports.

Titanium dioxide, which is one of the most basic materials in our daily life, has emerged as an excellent photocatalytic material for environmental protection [7]. However, pure titanium dioxide cannot satisfactorily fulfill the elevated activity demands for CO oxidation, and the manganese oxide could be a kind of active ingredient loading on it. To act as supports of catalysts, TiO₂ is widely used because it is cheap and non-toxic material. Usually commercial catalysts use common merchant TiO₂ as supports. But there are diverse kinds of TiO₂ supports with distinct preparation methods, especially mesoporous TiO₂ which have unique properties, in consequence of high surface area, controllable size and the highly ordered pore structure, extensive attentions have been concentrated in

✉ Runduo Zhang
zhangrd@mail.buct.edu.cn

¹ State Key Laboratory of Chemical Resource Engineering, Beijing University of Chemical Technology, 100029 Beijing, People's Republic of China

the synthesis and the application of mesoporous TiO_2 [8–10]. The large specific surface area and ordered porous frameworks make mesoporous oxides have a high activity and great adsorption capacity, and they have a potential application value in the fields of catalytic cracking and fine chemical industry because its large aperture [11]. TiO_2 has two common crystal phases, which are anatase and rutile, with different performances acting as supports [12, 13]. Since the sol–gel chemistry of titanium precursors is susceptible, the cooperative assembly is sensitive to variable reaction conditions. TiO_2 is an inert support which mainly provides the dispersing surface for the active component, by loading a certain amount of active substances on the mesoporous TiO_2 , the catalytic performance could be potentially improved.

Mesoporous materials are considered promising as high-efficiency catalysts due to their large pore sizes and high surface areas. Nanoparticles are used as building blocks instead of molecular precursors via the evaporation-induced self-assembly (EISA) method. Yang and Zhao et al. have developed a simple and general procedure for the synthesis of ordered mesoporous metal oxides, including TiO_2 , and those mesoporous metal oxides are formed through a mechanism that combines block copolymer self-assembly with alkylene oxide complexation of the inorganic metal species [14, 15]. This synthetic strategy reduced synthesis time and produced nanocrystalline frameworks under a mild calcination.

In this work, a series of TiO_2 oxides with diverse morphologies as supports of manganese species, as potential catalysts for CO oxidation reaction, is synthesized by different methods. These catalysts are characterized by XRD, N_2 adsorption–desorption, pore size distributions, TEM, H_2 -TPR and XPS to contrast their physicochemical properties and correlated with the corresponding catalytic performance.

Experimental

Catalysts preparation

TiO₂ supports

Six methods were used for the preparation of TiO_2 supports.

1. EISA (evaporation-induced self-assembly) method

1.6 g of F127 ($\text{EO}_{106}\text{PO}_{70}\text{EO}_{106}$), 2.3 mL of CH_3COOH , and 0.74 mL of HCl were dissolved in 30 mL of ethanol, and then 3.5 mL of TBOT (tetrabutyl titanate) was added to the above solution. The mixture was stirred vigorously for 1 h and transferred into a Petri dish to allow evaporation process at 40 °C with a relative humidity of

40 % for 2 days, transparent TiO_2 nanocomposites were formed and thereafter transferred into a 65 °C oven and aged for an additional 24 h. The as-made mesostructured hybrids were calcined under 350 °C for 4 h with rate 1 °C/min. The sample obtained was denoted as EISA.

2. Sol–gel method

0.75 g of CTAB ($\text{C}_{16}\text{H}_{33}(\text{CH}_3)_3\text{NBr}$) was dissolved in 25 g of isopropanol. 5 g TBOT, 1 mL CH_3COOH and 0.5 mL HCl were then added to the above solution, respectively. The mixture was stirred for 0.5 h to form homogeneous pale yellow solution A. 1.5 mL of deionized water was added to 2 mL isopropanol to form solution B. Solution B was slowly added to Solution A. and stirred for 2 h at 30 °C to form a uniform milky gel, then aged for 48 h, followed by drying at 100 °C in a Petri dish. The final product was calcined under 400 °C for 4 h. The sample obtained was denoted as SG.

3. Hydrothermal method

2 g of P123 ($\text{EO}_{20}\text{PO}_{70}\text{EO}_{20}$) was dissolved in 20 mL of ethanol, and then 7.5 mL of TBOT was slowly added, stirred for 0.5 h. The mixture was added to the solution mixed with ethanol and deionized water dropwise and then stirred for 1 h. The resulting solution was transferred to PTFE hydrothermal reactor for 2 h under 80 °C. The obtained product was filtered and washed by deionized water and ethanol for three times, dried at 60 °C. The precursor was calcined at 200 °C for 1 h, and continued at 350 °C for 2 h. The sample obtained was denoted as HY.

4. Anatase sample

A certain amount of TBOT was dissolved in ethanol, and then dried at 100 °C, followed by calcination under 400 °C for 2 h. The sample obtained was denoted as AN.

5. Rutile sample

A certain amount of TBOT was dissolved in ethanol, and then dried at 100 °C, followed by calcination under 800 °C for 2 h. The sample obtained was denoted as RU.

6. Hard templates method

TBOT was dissolved in ethanol under continuous stirring following by the addition deionized water dropwise into the solution until no more white precipitate of titanium hydroxide was produced. The white precipitate was recovered by filtering and washing with distilled water. After drying, 0.2 g of the precipitate was dissolved in 20 mL of HNO_3 solution (70 %) to form a 0.085 M titanium nitrate solution (calculated based on Ti ions). Subsequently, 0.15 g of SBA-15, prepared by a classic way, was mixed with the titanium nitrate solution under stirring for 2 h, and the mixed solution was transferred into a 50 mL crucible and dried at 40 °C. The dried white powder was placed in a muffle furnace for calcination. The as-made composite was mixed with 0.2 M NaOH solution at 80 °C under stirring for 2–3 min, this process was repeated once again. TiO_2 powder was washed with distilled water

twice, followed by drying at 40 °C [16]. The obtained sample was denoted as HT.

Metal loading

50 mL of demonized water was added to a beaker containing 1 g of support. The mixture was heated to 70 °C under continuous stirring. A measured quantity of manganese nitrate (mass fraction of manganese oxides is 2 %) was then added to the above solution, and the mixture was evaporated to eliminate the superfluous water. The obtained product was further dried overnight at 110 °C, and finally calcined at 400 °C for 2 h in air.

Catalysts characterization

X-ray diffraction (XRD)

X-ray powder diffraction patterns have been recorded with a Bruker D8 X-Ray diffractometer, which employed a Cu K α radiation ($\lambda = 0.15406$ nm). The scanning range 2θ was 10°–80° with a step size of 0.1° at the speed of 1 s/step.

Transmission electron microscopy (TEM)

Transmission electron microscopy (TEM) images were carried out using a JEM-3010 electron microscope, respectively. The samples were ultrasonically dispersed in ethanol and then were deposited over copper grid.

X-ray photoelectron spectroscopy (XPS)

X-ray photoelectron spectroscopy (XPS) data were conducted on a Thermo fisher ESCALAB 250 system with Al K α radiation as the X-ray source. The measurements were carried out in an ultrahigh vacuum (UHV) chamber. The sensitivity of ISS is 25 kcps/nA. And the binding energies (BE) were referenced to the carbon deposit C (1 s) line at 284.6 eV.

BET analysis

The specific surface areas (S_{BET}), pore size distributions, pore total volumes and sorption isotherms of the TiO₂ and the Mn/TiO₂ were measured by nitrogen physisorption at liquid nitrogen temperature (−196 °C) by the Brunauer–Emmett–Teller (BET) method using an automated gas sorption system (Sorpromatic 1990, Thermo Electron). Pore size distributions of the different catalysts were calculated according to the Barrett–Joyner–Halenda (BJH) model from the data of desorption branch of the nitrogen

isotherms. Micropore volume (V_{micro}) was obtained by using t-plot method.

Temperature-programmed reduction (TPR)

Temperature-programmed reduction by hydrogen (H₂-TPR) was conducted inside a fixed-bed reactor loading with about 50 mg samples. The catalyst samples were heated from 50 to 800 °C at a rate of 5 °C/min under a flow of 5 % H₂/Ar (40 mL/min). The consumption of hydrogen was on-line monitored by gas chromatography (GC 4000A) equipped with a thermal conductivity detector (TCD).

Catalytic activity tests

The catalytic performances of Mn/TiO₂ catalysts in the CO oxidation reaction have been investigated in a fixed-bed flow reactor using 200 mg of catalyst. The temperature was varying from 100 to 350 °C at ambient pressure. The total volumetric gas flow was 33.6 mL/min, which was the mixture of CO, O₂ and Ar. The proportion of CO is 1 % balanced by Ar.

Results and discussion

XRD, TEM, and BET analysis

Figure 1 shows the X-ray diffraction patterns of Mn/TiO₂ catalysts prepared through different methods with the same actual Mn loading, 2 %, the diffraction peaks of the materials of Mn/EISA, Mn/SG, Mn/HY, Mn/AN and Mn/HT appeared at $2\theta = 25.4^\circ, 37.8^\circ, 48.1^\circ, 54.0^\circ, 55.1^\circ$ and

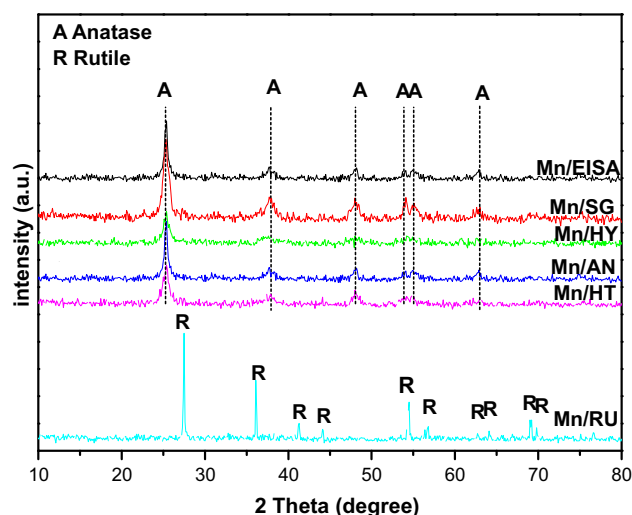


Fig. 1 The XRD patterns of Mn/TiO₂ catalysts prepared by different methods

62.8° corresponding to lattice plane (1 0 0), (0 0 4), (2 0 0), (1 0 5), (2 1 1) and (2 0 4), respectively. These were accordingly assigned to anatase crystal phase of TiO₂ (JCPDS 21-1272). Mn/RU sample was similar to the rutile TiO₂ (JCPDS 21-1276). As shown in Fig. 1 the diffraction peaks assigned to crystalline manganese oxide species are very weak, indicating that the Mn ions are well dispersed on TiO₂ supports in amorphous state. Yue et al. [17] mentioned that the crystal phase and mesoporous structure of TiO₂ highly dependent on the calcination temperature thence TiO₂ supports made in the temperature range of 350–800 °C showed different diffraction peaks. According to the diffraction peak intensities, the Mn/RU catalyst showed the better crystallinity phase due to its high calcination temperature, whereas the Mn/HY showed the worst crystallization.

In Fig. 2 the textural properties are investigated by N₂ physical sorption, representing a typical feature of mesoporous materials for all prepared Mn/TiO₂ catalysts except the catalyst with RU support. These calcined samples exhibit a type IV curve. Mn/EISA featuring a H2 hysteresis loop, suggests that it has a uniform size and shape. Others exhibit a H1 hysteresis loop, suggesting that they have a non-uniform structure. Michal Kruk et al. [18] have found that the position of the capillary condensation step gradually shifts to higher relative pressures and the relative height of the capillary condensation step increases with increasing pore diameter, which means Mn/EISA may has the largest pore diameter. An initial increase in adsorption capacity is assigned to monolayer adsorption on the micropore surface as well as monolayer and initial multilayer adsorption in the mesopore intrawall at relatively lower pressures ($P/P_0 < 0.1$). Subsequently, the upward deviation at higher P/P_0 (0.4–0.8) is believed to be associated with the progressive filling of mesopores via capillary condensation [19]. All the catalysts

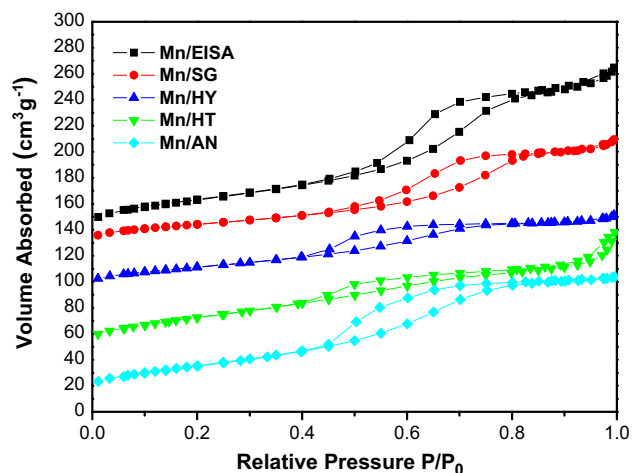


Fig. 2 Nitrogen adsorption/desorption isotherms of Mn/TiO₂ catalysts prepared by different methods

still kept mesoporous structure after the deposition of manganese oxide species and the subsequent calcination, indicating that the catalysts have a good stability. Figure 3 presents the pore size distributions of samples, which obviously showed the largest pore size of Mn/EISA, which it is agreed with the result in Fig. 2.

BET specific surface areas, average pore diameter (D_a), most probable pore diameter (D_m), crystallite size of TiO₂ supports, and pore size distributions of the various Mn/TiO₂ catalysts are shown in Table 1 and Fig. 3. These samples with mesoporous structure have larger surface areas than the other samples. BET surface area of both the supports and the catalysts (with corresponding supports) decrease in the following order: EISA > HY > AN > SG > HT > RU. The EISA sample shows the highest surface area (217.14 m²/g) due to its regular mesoporous structure. Moreover, RU sample has the lowest surface area and the largest crystallite size in consequence of feature of crystallite phase. Compared with pure TiO₂ supports, the BET surface areas of Mn/TiO₂ decrease rapidly with an introduction of 2 % Mn indicating that the loading an active ingredient on the channel of the TiO₂ support could reduce the free volume and surface area of the result catalyst. The surface area of catalyst with EISA support decreases in a manner more significantly after loading Mn component as compared to other catalysts due to its mesoporous structure of the supports; it is not as stable as others [20]. The mesoporous Mn/EISA has the largest pore size along with not only the average pore diameter, but also the most probable pore diameter, which corresponds to the pore size distributions (Fig. 3). After loading the active component, the pore diameter of the EISA samples increased, suggesting that the micropores of the supports are plugged. The smallest pore sizes (4.2 nm) are observed for RU samples, which would likely limit the

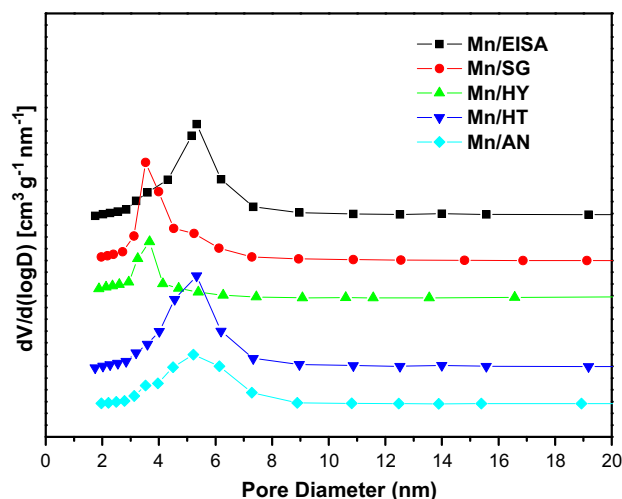


Fig. 3 Pore size distributions of Mn/TiO₂ catalysts prepared by different methods

Table 1 BET surface area, average pore diameter, most probable pore diameter and particle size of various Mn/TiO₂ catalysts

Catalysts	S _{BET} ^a (m ² /g)	S _{BET} ^b (m ² /g)	Da ^a (nm)	Dm ^a (nm)	Da ^b (nm)	Dm ^b (nm)	Particle size (nm)
Mn/EISA	217.1	120.2	5.5	4.2	6.5	5.3	7.5
Mn/SG	109.1	70.5	7.0	5.0	5.4	3.5	9.0
Mn/HY	122.7	78.1	5.2	3.9	4.6	3.7	8.1
Mn/HT	119.0	64.2	4.2	3.2	2.5	5.2	8.9
Mn/AN	112.2	75.6	5.4	3.3	4.1	5.2	9.8
Mn/RU	24.1	4.5	–	–	–	–	64.1

^a According to XRD results of the TiO₂ supports

^b According to estimation from nitrogen adsorption of Mn/TiO₂ catalysts

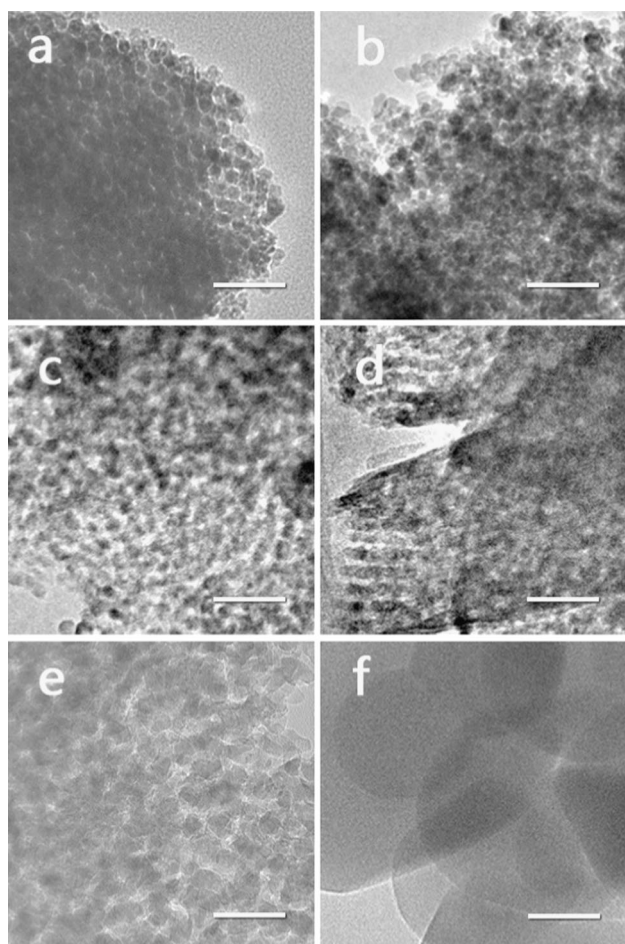


Fig. 4 TEM images of the TiO₂ samples. **a** EISA, **b** HY, **c** SG, **d** HT, **e** AN, **f** RU. Scale bar 50 nm

introduction of Mn species into the pore channel of TiO₂ supports and further distribution.

TEM images illustrate the morphology of the TiO₂ supports prepared via different methods in Fig. 4. Manganese oxides are hardly distinguishable from TEM image when the loading amount of Mn on various TiO₂ supports, suggesting that the Mn species are highly dispersed

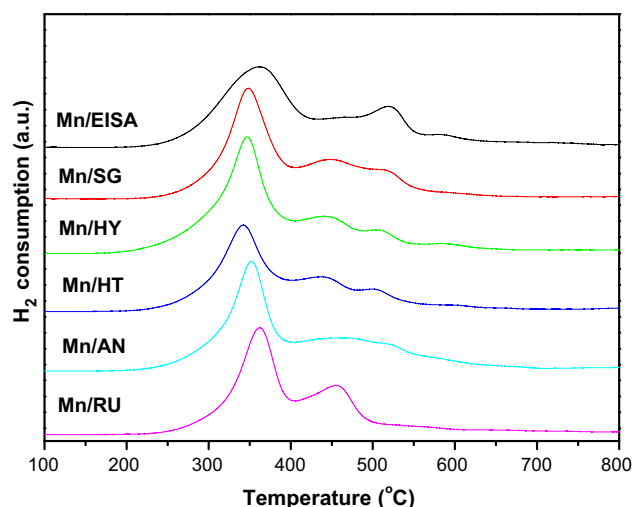


Fig. 5 H₂-TPR profiles of Mn/TiO₂ catalysts

compared to the limit detection by XRD (Fig. 1). EISA samples show highly ordered mesoporous channels that presented in large domain, effectively enlarging the BET surface area (Table 1), which are similar to the cubic bicontinuous (*Ia3d*) textures. Only worm-like structure can be found in SG and HY samples. This worm-like structure is sometime more stable than ordered structure, which is already shown in Table 1, the above results well agree with what is mentioned in early literature [21, 22]. As described in the literature previously [23], HT sample shows a partial regular and replicated structure. The particles of RU samples are huge and relatively independent, which coincides with its large crystallite size (Table 1).

H₂-TPR analysis

The temperature-programmed reduction profiles of various manganese supported on TiO₂ catalysts are shown in Fig. 5. TPR experiments are performed on pure TiO₂, no noticeable H₂ consumption is observed for these samples under 800 °C. Thus, the H₂ consumption detected for

Fig. 6 The curve-fitted Mn 2p_{3/2} XPS spectra of various Mn/TiO₂ catalysts

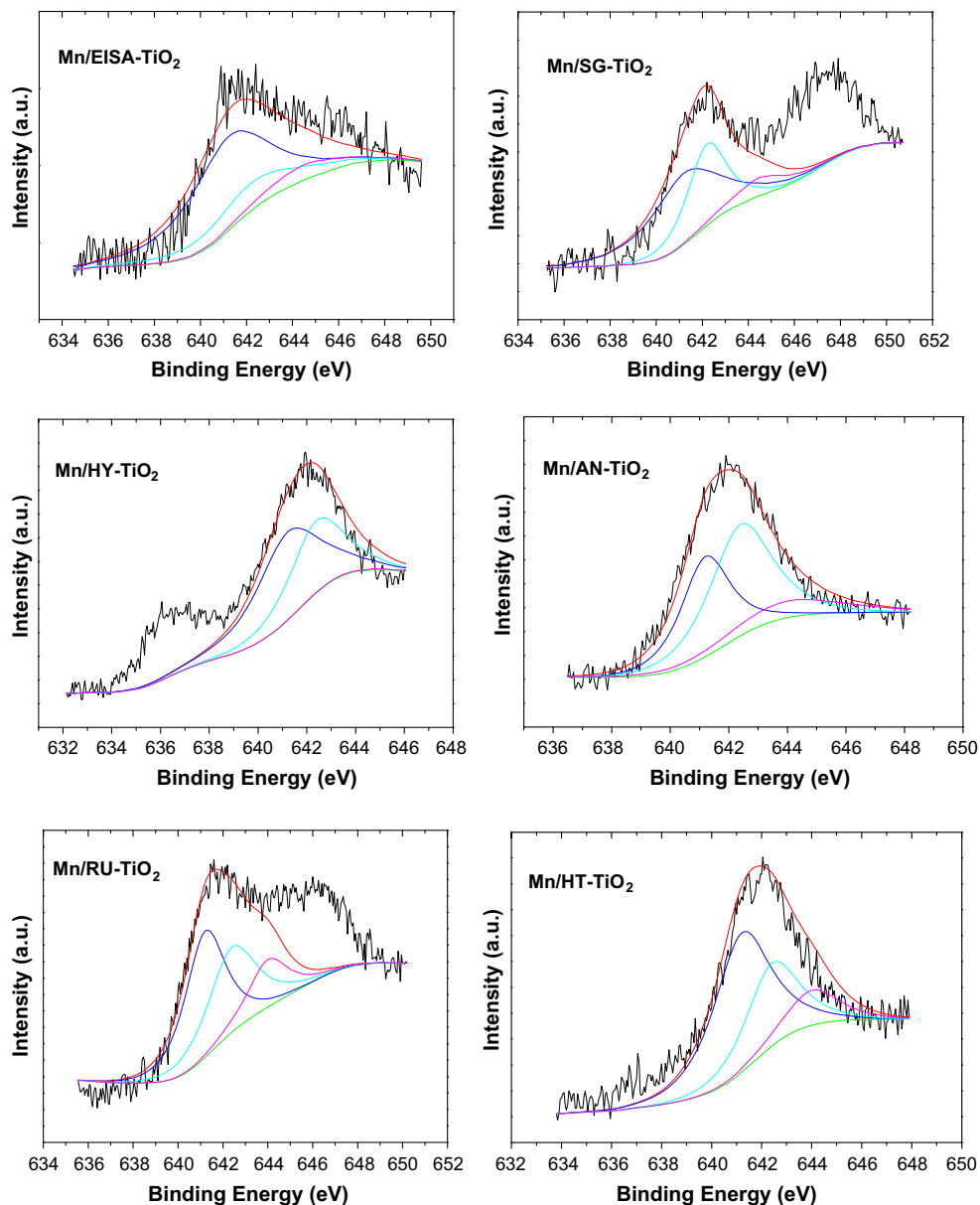


Table 2 XPS data of Mn/TiO₂ catalysts with different supports

Catalysts	Mn ²⁺ (%)	Mn ³⁺ (%)	Mn ⁴⁺ (%)
Mn/EISA	10	68	22
Mn/SG	9	56	35
Mn/HY	3	56	41
Mn/HT	13	56	31
Mn/AN	14	36	50
Mn/RU	24	43	33

various Mn/TiO₂ catalysts primarily originates from the reduction of the manganese oxides species. It has been mentioned that the low temperature peaks are on account of highly dispersed metal oxide particles on the supports and

the second reduction peak is typically assigned to the hydrogen consumed in the reaction with sub-surface lattice oxygen, which could migrate from the interior to the surface of the catalyst at higher temperatures [24].

From the present H₂-TPR profiles, it was obvious that there were three reduction steps: MnO₂ to Mn₂O₃, Mn₂O₃ to Mn₃O₄, and Mn₃O₄ to MnO [25]. Whereas each kind of MnO_x favored its corresponding peaks, it was difficult to identify the MnO_x species consistent with the TPR profiles, considering the investigated above. For Mn/EISA catalysts, the intensity of the first reduction peak is smaller than other catalysts, which is probably due to the strong interaction between MnO_x and TiO₂. Based on previous literature [26], the highly dispersed MnO_x might be the precursor of the

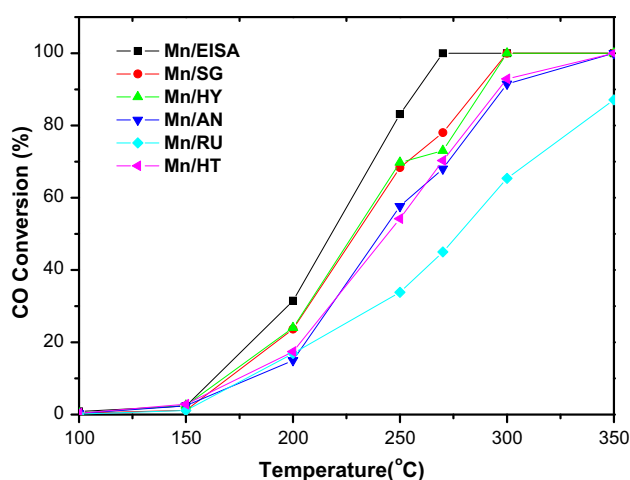


Fig. 7 CO conversion over the Mn/TiO₂ catalysts prepared by different methods

active phase and provide active sites. These results were in good agreement with the XRD and TEM results.

XPS analysis

Despite the six catalysts being prepared through different methods using equal concentrations of Mn supporting on TiO₂, the Mn 2p_{3/2} XPS spectra of Mn/TiO₂ samples were conducted and surface atomic ratios were calculated (Fig. 6; Table 2), which evaluates the oxidation state and interaction between Mn species and TiO₂ supports. Through performing curve-fitting deconvolution, the Mn 2p_{3/2} spectra could be separated into three peaks showed contributions referenced to Mn²⁺ (644 ± 0.2 eV), Mn³⁺ (641.2 ± 0.2 eV) and Mn⁴⁺ (642.7 ± 0.2 eV) [27, 28]. The spectra indicate that Mn/EISA could enhance its catalytic performance from the enriched MnO_x species on surface acting as proper active sites. Depending on Table 2, it is obvious that the main ion is Mn³⁺ for all catalysts except Mn/AN. Mn/EISA sample contained approximately 68 % Mn³⁺ species, more than in other catalysts. Mn³⁺ is a significant contributor to the number of active sites for catalytic CO oxidation and thus improving the catalytic performance.

Catalytic activity

Figure 7 shows the variation of CO conversion as a function temperature for Mn/TiO₂ catalysts synthesized using different methods. The catalytic behavior has been correlated with the results of specific surface area and structure properties. The catalyst with EISA-TiO₂ support, which reveals the highest specific surface area and smaller crystallite size with highly ordered mesoporous structure,

shows the highest catalytic activity among the catalyst with SG, HY, HT and RU supports; 100 % conversion is achieved at 270 °C. So, the EISA method is chosen to prepare TiO₂, which could support the Mn species as active component in highly dispersed state, suggesting that the MnO_x has strong interaction with TiO₂ support which effectively improves the catalytic performance of CO oxidation reaction.

Conclusion

A series of Mn/TiO₂ catalysts has been prepared and investigated for the catalytic CO oxidation reaction. Comparing Mn/TiO₂ catalysts with different kind of supports, it is found that the catalyst with TiO₂ support made by EISA method exhibits the best catalytic activity for CO oxidation especially at low temperature. XRD and TPR results indicated that the highly dispersed MnO_x were in amorphous state. TEM results worked in concert with the BET results and showed the highly ordered mesoporous structure catalyst with EISA-TiO₂ support, which effectively enlarges the surface area, leading to promoting strong interactions between Mn species as active component and TiO₂ supports. XPS studies indicated the effect of valence of Mn, in which Mn³⁺ was a significant contributor to the number of active sites for CO oxidation reaction and thus benefited the catalytic performance.

Open Access This article is distributed under the terms of the Creative Commons Attribution 4.0 International License (<http://creativecommons.org/licenses/by/4.0/>), which permits unrestricted use, distribution, and reproduction in any medium, provided you give appropriate credit to the original author(s) and the source, provide a link to the Creative Commons license, and indicate if changes were made.

References

- Li X, Zhang Sh, Jia Y, Liu X, Zhong Q (2012) Selective catalytic oxidation of NO with O₂ over Ce-doped MnO_x/TiO₂ catalysts. *Nat Gas Chem* 21:17–24
- Murray JW (1975) The interaction of metal ions at the manganese dioxide-solution interface. *Geochim Cosmochim Acta* 39:505–519
- O'Reilly SE, Hochella MF Jr (2003) Lead sorption efficiencies of natural and synthetic Mn and Fe-oxides. *Geochim Cosmochim Acta* 67:4471–4487
- Stumm W, Giovanoli R (1976) Nature of particulate manganese in simulated lake waters. *New Swiss Chemical Soc C/O Novartis AG, K-25 1 45, CH-4002 BASEL, Switzerland*, pp 423–425
- Geesey GG, Neal AL, Suci PA, Peyton BM (2002) A review of spectroscopic methods for characterizing microbial transformations of minerals. *J Microbiol Methods* 51:125–139
- Kim HY, Lee HM, Pala RGS, Shapovalov V, Metiu H (2008) CO Oxidation by Rutile TiO₂ (110) Doped with V, W, Cr, Mo, and Mn. *J Phys Chem C* 112:12398–12408

7. Kumaresan L, Mahalakshmi M, Palanichamy M, Murugesan V (2010) Synthesis, characterization, and photocatalytic activity of Sr^{2+} doped TiO_2 nanoplates. *Ind Eng Chem Res* 49:1480–1485
8. Burda C, Chen X, Narayanan R, El-Sayed MA (2005) Chemistry and properties of nanocrystals of different shapes. *Chem Rev* 105:1025–1102
9. Stark WJ, Wegner K, Pratsinis SE, Baiker A (2001) Flame aerosol synthesis of vanadia-titania nanoparticles: structural and catalytic properties in the selective catalytic reduction of NO by NH_3 . *J Catal* 197:182–191
10. Zallen R, Moret M (2006) The optical absorption edge of brookite TiO_2 . *Solid State Commun* 137:154–157
11. Husain A, Huss Jr A, Klocke DJ, Timken HK (1993) Isoparaffin: olefin alkylation in the presence of synthetic porous MCM-49. US Patent 5,254,792: Google Patents
12. Bakaev V, Steele W (1992) Computer simulation of the adsorption of argon on the surface of titanium dioxide. 1. Crystalline rutile. *Langmuir* 8:1372–1378
13. Xu Y, Chen W-K, Liu S-H, Cao M-J, Li J-Q (2007) Interaction of photoactive catechol with TiO_2 anatase (101) surface: a periodic density functional theory study. *Chem Phys* 331:275–282
14. Yang P, Zhao D, Margolese DI, Chmelka BF, Stucky GD (1998) Generalized syntheses of large-pore mesoporous metal oxides with semicrystalline frameworks. *Nature* 396:152–155
15. Yang P, Zhao D, Margolese DI, Chmelka BF, Stucky GD (1999) Block copolymer templating syntheses of mesoporous metal oxides with large ordering lengths and semicrystalline framework. *Chem Mater* 11:2813–2826
16. Kota AS, Luss D, Balakotaiah V (2012) Modeling studies on lean NO_x reduction by a sequence of LNT–SCR bricks. *Ind Eng Chem Res* 51:6686–6696
17. Ozawa M, Seo Y, Yukimura A, Ueda Y (1999) Recent Technology for IHI Denitrification (SCR) System. *Ishikawajima Harima Eng Rev* 39:356
18. Kruk M, Jaroniec M (2000) Accurate method for calculating mesopore size distributions from argon adsorption data at 87 K developed using model MCM-41 materials. *Chem Mater* 12:222–2230
19. Hoang V-T, Huang Q, Eic M, Do T-O, Kaliaguine S (2005) Structure and diffusion characterization of SBA-15 materials. *Langmuir* 21:2051–2057
20. Kapoor MP, Inagaki S, Yoshida H (2005) Novel zirconium-titanium phosphates mesoporous materials for hydrogen production by photoinduced water splitting. *J Phys Chem B* 109:9231–9238
21. Chen L, Yao B, Cao Y, Fan K (2007) Synthesis of well-ordered mesoporous titania with tunable phase content and high photoactivity. *J Phys Chem C* 111:11849–11853
22. Lu Y, Yuan M, Liu Y, Tu B, Xu C, Liu B et al (2005) Photoelectric performance of bacteria photosynthetic proteins entrapped on tailored mesoporous WO_3 – TiO_2 films. *Langmuir* 21:4071–4076
23. Yue W, Xu X, Irvine JT, Attidekou PS, Liu C, He H et al (2009) Mesoporous monocrystalline TiO_2 and its solid-state electrochemical properties. *Chem Mater* 21:2540–2546
24. Doggali P, Teraoka W, Mungse P, Shah IK, Rayalu S, Labhsetwar N (2012) Combustion of volatile organic compounds over Cu–Mn based mixed oxide type catalysts supported on mesoporous Al_2O_3 , TiO_2 and ZrO_2 . *J Mol Catal A Chem* 358:23–30
25. Fang D, Xie J, Hu H, Yang H, He F, Fu ZH (2015) Identification of MnO_x species and Mn valence states in $\text{MnO}_x/\text{TiO}_2$ catalysts for low temperature SCR. *Chem Eng J* 271:23–30
26. Li W, Zhuang M, Xiao T, Green M (2006) MCM-41 supported Cu–Mn catalysts for catalytic oxidation of toluene at low temperatures. *J Phys Chem B* 110:21568–21571
27. Ko JH, Park SH, Jeon J-K, Kim S-S, Kim SC, Kim JM et al (2012) Low temperature selective catalytic reduction of NO with NH_3 over Mn supported on $\text{Ce}_{0.65}\text{Zr}_{0.35}\text{O}_2$ prepared by supercritical method: effect of Mn precursors on NO reduction. *Catal Today* 185:290–295
28. Park E, Chin S, Jeong J, Jung Jongsoo (2012) Low-temperature NO oxidation over Mn/ TiO_2 nanocomposite synthesized by chemical vapor condensation: effects of Mn precursor on the surface Mn species. *Microporous Mesoporous Mater* 163:96–101